nature communications

Article

https://doi.org/10.1038/s41467-025-62276-x

Microscopic theory of polariton group velocity renormalization

Received: 3 February 2025

Accepted: 17 July 2025

Published online: 29 July 2025

Check for updates

Wenxiang Ying [1,6], Benjamin X. K. Chng [2,6], Milan Delor [3] & Pengfei Huo [1,4,5]

Cavity exciton-polaritons exhibit ballistic transport and can achieve 100 μm in one picosecond. This ballistic transport significantly enhances mobility compared to that of bare excitons, which often move diffusively and become the bottleneck for energy conversion and transfer devices. Despite being robustly reproduced in experiments and simulations, there is no microscopic theory available for describing the group velocity v_g of polariton transport and its renormalization. In this work, we derive an analytic expression for v_g renormalization. The theory suggests the v_g renormalization is caused by phonon-mediated transitions between the lower polariton (LP) states and the dark states. The theory predicts that the renormalization magnitude depends on both exciton-phonon coupling strength and temperature, which are in quantitative agreement with numerical quantum dynamics simulations. Our results provide theoretical insights and a predictive analytical theory for understanding cavity-enhanced exciton-polariton transport.

Recent experiments[1–7] have shown that exciton transport in semiconductors can be significantly enhanced by coupling these excitons to confined electromagnetic modes inside an optical cavity. By forming cavity exciton-polaritons, the electronic excitation is capable of traversing long distances ballistically at a high group velocity v_g. This novel strategy of cavity-enhanced ballistic exciton energy transport[4] allows devices to bypass the intrinsic bottleneck of diffusive transport, offering a paradigm shift in fundamental energy science and device applications such as halide perovskite solar cells[1,8] and light-emitting diode displays[9–11]. The high group velocity mainly arises from the large gradient of the dispersion curve of the polariton bands (compared to the pure-matter band). Multiple recent experiments that image polariton propagation[3,4,6,7,12] have observed polariton group velocities that are substantially lower than expected from their dispersion. This deviation, often referred to as group velocity renormalization, is particularly noticeable for polaritons with large excitonic fractions[4,6,13].

Recent progress in the theoretical understanding of polariton transport[2,14–21] have emerged through numerical simulations[6,20–22] and theoretical models[6,15,16], providing valuable insights into this complex phenomenon. In the framework of theoretical models, two prevailing hypotheses for v_g renormalization have been presented. One is the thermally activated scattering theory (TAST) in ref. 6, which posits that there will be a quasi-equilibrium between the polariton band and the dark exciton states. Under this theory, ballistic transport occurs only during the period when the system is in the polariton band (see the details of the theory in the Supplementary Information of ref. 6). As such, v_g is reduced, and the extent of the renormalization depends on the energy difference between the polariton band and the dark excitons. A similar hypothesis is also proposed in ref. 3. The second hypothesis is the transient localization hypothesis proposed in ref. 4, which arises from the interpretation of trajectory results in the Ehrenfest mixed-quantum-classical (MQC) simulations. According to this hypothesis, the polariton wavepacket predominantly exhibits ballistic coherent transport, but the wavepacket becomes transiently localized due to phonon coupling, manifested by thermally activated displacements of nuclear coordinates. A detailed ab-initio mixed quantum-classical study that supports both of the above-mentioned mechanisms can be found in ref. 20. This hypothesis explains the

[1]Department of Chemistry, University of Rochester, Rochester, NY, USA. [2]Department of Physics and Astronomy, University of Rochester, Rochester, NY, USA. [3]Department of Chemistry, Columbia University, New York, NY, USA. [4]The Institute of Optics, Hajim School of Engineering, University of Rochester, Rochester, NY, USA. [5]Center for Coherence and Quantum Science, University of Rochester, Rochester, NY, USA. [6]These authors contributed equally: Wenxiang Ying, Benjamin X. K. Chng. e-mail: pengfei.huo@rochester.edu

group velocity renormalization and the ballistic transport concurrently and can be examined from the trajectories obtained from the mixed quantum-classical simulations directly. Despite these promising developments, there is no microscopic theory, to the best of our knowledge, that quantitatively describes v_g-renormalization and shows how v_g-renormalization depends on exciton-phonon coupling (reorganization energy λ), temperature T, exciton fraction in the polariton, etc.

In this work, we develop a microscopic theory using a field-theoretic approach to explain the polariton v_g-renormalization due to polariton-phonon interactions. By utilizing the polariton Green's functions, we derive the modified band structure for polaritons, which results in a renormalized polariton group velocity. Our theory indicates that within the lower polariton (LP) branch, the system manifests a dark state manifold-mediated scattering process due to phonons, thus slowing down the band-like transport. The theory predicts that the extent of modification scales linearly with the phonon bath reorganization energy λ, and similarly, displays a linear temperature dependence in the high-temperature regime. We also show that the theoretical predictions are in quantitative agreement with numerical results based on MQC simulations[21].

Results and discussions

Model system

We use the Generalized Holstein-Tavis-Cummings (GHTC) Hamiltonian[23–26] to describe N excitons interacting with $\mathcal{M}$ cavity modes, and $N \gg \mathcal{M}$ in line with typical experimental conditions. Typically, one estimates $N/\mathcal{M} \sim 10^6 - 10^9$ for systems used in experiments[27]. The total Hamiltonian can be written in the form of the system-bath model and is expressed as $\hat{H} = \hat{H}_S + \hat{h}_B + \hat{H}_{SB}$. The system Hamiltonian $\hat{H}_S$ consists of the excitonic degrees of freedom (DOF) and the photonic DOF of the cavity. Each exciton is modeled as an effective two-level system that consists of the ground state $|g_n\rangle$ and excited state $|e_n\rangle$ (for the n_{th} exciton). Without making the long-wavelength approximation[26], $\hat{H}_S$ is expressed as follows,

$$\begin{aligned}\hat{H}_S = \hbar\omega_0 \sum_{n=1}^{N} \hat{\sigma}_n^\dagger \hat{\sigma}_n + \sum_{k}^{\mathcal{M}} \hbar\omega_k \hat{a}_k^\dagger \hat{a}_k \\ + \sum_k \sum_{n=1}^{N} \hbar g_k \left[\hat{a}_k^\dagger \hat{\sigma}_n e^{-ik_\parallel \cdot x_n} + \hat{\sigma}_n^\dagger \hat{a}_k e^{ik_\parallel \cdot x_n} \right],\end{aligned} \tag{1}$$

where $\hat{\sigma}_n^\dagger = |e_n\rangle\langle g_n|$ and $\hat{\sigma}_n = |g_n\rangle\langle e_n|$ are the creation and annihilation operators of the n_{th} molecule's exciton, and ω_0 is the excitation energy between the molecule's ground and excited state. Furthermore, $\hat{a}_k$ and $\hat{a}_k^\dagger$ are the photonic field annihilation and creation operators for mode k whose frequency is ω_k. Note that the GHTC model described here does not contain exciton inter-site hopping or exciton-exciton interactions, which might prove to be important for a realistic description of polariton transport.

For Fabry–Pérot (FP) cavities, the dispersion is

$$\omega_k(k_\parallel) = c\sqrt{k_\perp^2 + k_\parallel^2}, \tag{2}$$

where c is the speed of light in vacuum. When $k_\parallel = 0$, the photon frequency is $\omega_c \equiv \omega_k(k_\parallel = 0) = ck_\perp$. The second line of Eq. (1) represents light-matter interaction, where $g_k = g_c\sqrt{(\omega_k/\omega_c)}\cos\theta$ is the k-dependent light-matter coupling strength[4], and $\tan\theta = k_\parallel/k_\perp$ is the incident angle. Note that the θ angle inside the cavity differs from the angle of incidence outside the cavity if the cavity background refractive index is not 1. Furthermore, x_n is the position of the n_{th} exciton. We consider the cavity modes inside the same simulation box as the excitons, with total size NL along the $k_\parallel$ direction ($L = x_n - x_{n-1}$).

As such, $k_\parallel$ has discrete (but quasi-continuous) values of $k_\parallel = \frac{2\pi}{NL}k$, where the mode index is $k \in [-\frac{\mathcal{M}-1}{2}, \ldots 0, \ldots \frac{\mathcal{M}-1}{2}]$. Diagonalizing $\hat{H}_S$ in the singly excited subspace leads to $2\mathcal{M}$ polariton states $|\pm_k\rangle$, with eigen-energies

$$\epsilon_{\pm k} = \hbar\omega_{\pm k} = \frac{\hbar}{2}(\omega_k + \omega_0) \pm \frac{\hbar}{2}\sqrt{(\omega_k - \omega_0)^2 + 4Ng_k^2}, \tag{3}$$

where $+$ and $-$ denote the upper polariton (UP) and LP branches, respectively. In addition, there are $N - \mathcal{M}$ dark states $|\mathcal{D}_k\rangle$ with energies $\hbar\omega_{\mathcal{D}k} = \hbar\omega_0$, which do not mix with photonic states and form the dark exciton branch. The definition of these dark states is provided in Supplementary Note 1.

Under the polariton representation, the system Hamiltonian in Eq. (1) is expressed as $\hat{H}_S = \sum_{\mu,k}\hbar\omega_{\mu k}\hat{P}_{\mu,k}^\dagger\hat{P}_{\mu,k}$, where $\hat{P}_{\mu,k}^\dagger$, $\hat{P}_{\mu,k}$ are the polariton creation and annihilation operators for polariton state k on polariton band μ, respectively, and the band label $\mu \in \{+, -, \mathcal{D}\}$. Specifically,

$$\hat{P}_{+,k}^\dagger = \cos\Theta_k\hat{B}_k^\dagger + \sin\Theta_k\hat{a}_k^\dagger \tag{4a}$$

$$\hat{P}_{-,k}^\dagger = -\sin\Theta_k\hat{B}_k^\dagger + \cos\Theta_k\hat{a}_k^\dagger, \tag{4b}$$

where $\hat{B}_k^\dagger = (1/\sqrt{N})\sum_{n=1}^{N} e^{-ik_\parallel\cdot x_n}\hat{\sigma}_n^\dagger$ creates the collective bright excitons, and

$$\Theta_k = \frac{1}{2}\arctan\left(\frac{2\sqrt{N}g_k}{\omega_k - \omega_0}\right) \in \left[0, \frac{\pi}{2}\right) \tag{5}$$

is the mixing angle. Details on the derivation in the polariton representation, as well as the expressions of the polariton operators, are provided in Supplementary Note 1. We present a schematic illustration

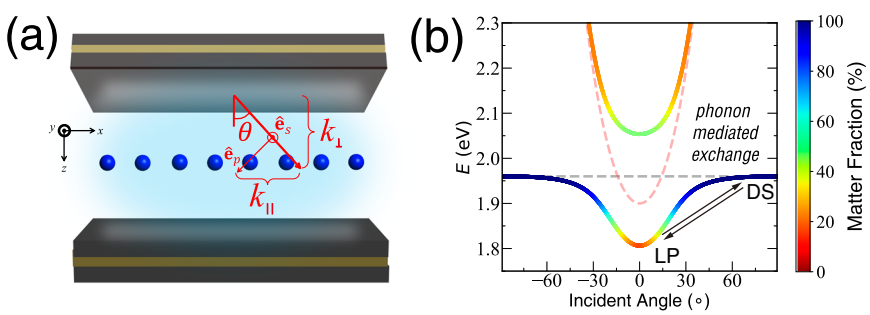

Fig. 1 | Schematics of the GHTC model and band structure. a Schematics of the model setup. Inside an optical cavity, the separated molecules collectively interact with many cavity modes. **b** Polariton band structure, where the matter fraction is shown in terms of the colorbar. The dashed lines are the bare photon (red) and matter (silver) dispersions, respectively. The phonon-mediated exchange effect between the lower polariton (LP) and the dark states (DS) manifold is also indicated, which is the main cause of polariton group velocity renormalization.

of the model system above, as well as the polariton band structure, in Fig. 1. Without coupling to phonons, the polariton exhibits band-like transport characterized by the group velocity

$$v_{g,\pm}(k_\parallel) = d\omega_{\pm k}/dk_\parallel, \tag{6}$$

where the $k_\parallel$-dependence of $\omega_{\pm k}$ is carried by ω_k via Eq. (2).

The bath Hamiltonian $\hat{h}_B$ describes the nuclear DOF, which we assume is a phonon environment that consists of a set of non-interacting harmonic oscillators, $\hat{h}_B = \sum_{n=1}^{N}\sum_\alpha \hbar\omega_\alpha \hat{b}^\dagger_{\alpha,n}\hat{b}_{\alpha,n}$, where $\hat{b}_{\alpha,n}$, $\hat{b}^\dagger_{\alpha,n}$ are the α_{th} bosonic bath phonon annihilation and creation operators in the n_{th} molecule with phonon frequency ω_α. Furthermore, $\hat{H}_{SB}$ describes the exciton-phonon interaction $\hat{H}_{SB} = \sum_{n=1}^{N}\hat{\sigma}^\dagger_n\hat{\sigma}_n \otimes \sum_\alpha c_\alpha(\hat{b}_{\alpha,n} + \hat{b}^\dagger_{\alpha,n})$, where c_α is the exciton-phonon coupling strength. We assume the coupling strength is identical for all excitons and c_α is therefore independent of the label n. Based on the Caldeira–Leggett model[28,29], the baths as well as their interactions with the system are described by the spectral density

$$J(\omega) = \frac{\pi}{\hbar}\sum_\alpha c_\alpha^2\delta(\omega-\omega_\alpha), \tag{7}$$

and $\lambda = (1/\pi)\int_0^{+\infty} d\omega\, J(\omega)/\omega = \sum_\alpha c_\alpha^2/\omega_\alpha$ is the reorganization energy.

We further introduce the Fourier transform of the bath phonon operators $\hat{b}_{\alpha,k} = (1/\sqrt{N})\sum_{n=1}^{N} e^{ik_\parallel\cdot x_n}\hat{b}_{\alpha,n}$. Using these transforms, the bath Hamiltonian is expressed as $\hat{h}_B = \sum_k\sum_\alpha \hbar\omega_\alpha \hat{b}^\dagger_{\alpha,k}\hat{b}_{\alpha,k}$, and the polariton-phonon interaction Hamiltonian is given by

$$\hat{H}_{SB} = \sum_{\mu,k,\nu,k'} \zeta_{\mu k}\cdot\zeta_{\nu k'}\hat{P}^\dagger_{\mu,k}\hat{P}_{\nu,k'}\sum_\alpha \frac{c_\alpha}{\sqrt{N}}\left(\hat{b}_{\alpha,k-k'} + \hat{b}^\dagger_{\alpha,k'-k}\right), \tag{8}$$

where the band labels $\mu,\nu \in \{+,-,\mathcal{D}\}$, and $\zeta_{\mu k}$ is a state-dependent coefficient that characterizes the matter fraction of the polariton state, with $\zeta_{+k} = \cos\Theta_k$ and $\zeta_{-k} = \sin\Theta_k$. The ζ_{+k} and ζ_{-k} are commonly referred to as the Hopfield coefficients[24,30,31], and we note that $\zeta_{\mathcal{D}k} = 1$. These polariton-phonon interactions will modify the polariton band structure, and will, in turn, affect the polariton transport properties such as the group velocity in Eq. (6).

Theory

We derive the expression for v_g-renormalization using the equilibrium Green's functions at finite temperature. We restrict our discussions to polariton transport in the weak exciton-phonon coupling regime and the band-like transport regime[4,6]. The single-particle Green's function of the polaritons at finite temperature is expressed as follows[32],

$$G_{\mu,k}(t) \equiv -i\theta(t)\langle \hat{P}_{\mu,k}(t)\hat{P}^\dagger_{\mu,k}(0)\rangle, \tag{9}$$

where $\theta(t)$ is the Heaviside step function, the time-dependence of the operators read as $\hat{P}_{\mu,k}(t) = e^{\frac{i}{\hbar}\hat{H}t}\hat{P}_{\mu,k}(0)e^{-\frac{i}{\hbar}\hat{H}t}$, and $\langle\hat{A}\rangle \equiv \text{Tr}[\hat{A}e^{-\beta\hat{H}}]/\text{Tr}[e^{-\beta\hat{H}}]$ denotes the thermal average under finite temperature $\beta \equiv 1/(k_B T)$, where k_B is the Boltzmann constant. Similarly, one defines the Green's function of the phonons as $D_q(t) \equiv -i\sum_\alpha(c_\alpha^2/N)\cdot\langle\mathcal{T}(\hat{b}_{\alpha,q}(t) + \hat{b}^\dagger_{\alpha,-q}(t))(\hat{b}_{\alpha,-q}(0) + \hat{b}^\dagger_{\alpha,q}(0))\rangle$, where $\mathcal{T}$ is the time-ordering operator. The Green's function in Eq. (9) can be determined by the self-consistent Dyson equation in the time domain as[32]

$$\left(i\hbar\frac{\partial}{\partial t} - \epsilon_{\mu k}\right)G_{\mu,k}(t) - \int_0^t d\tau\,\Sigma_{\mu,k}(t-\tau)G_{\mu,k}(\tau) = \delta(t), \tag{10}$$

where $\Sigma_{\mu,k}(t)$ is the self-energy, and $\epsilon_{\mu k} = \hbar\omega_{\mu k}$ is the bare polariton energy. Eq. (10) is recast in the frequency domain as

$$\mathcal{G}^{-1}_{\mu,k}(\omega) = \hbar(\omega - \omega_{\mu k} + i\eta) - \Sigma_{\mu,k}(\omega), \tag{11}$$

where $\mathcal{G}_{\mu,k}(\omega)$ is the Fourier transform of $G_{\mu,k}(t)$, and we take $\eta \to 0_+$. To obtain the polariton band renormalization, we further define the renormalized polariton energies $\tilde{E}_{\mu k} = E_{\mu k} + i\Gamma_{\mu k}$ and plug it into Eq. (11), arriving at the expression[33]

$$E_{\mu k} = \hbar\omega_{\mu k} + \text{Re}\,[\Sigma_{\mu,k}(\tilde{E}_{\mu k}/\hbar)], \tag{12}$$

$$\Gamma_{\mu k} = \text{Im}\,[\Sigma_{\mu k}(\tilde{E}_{\mu k}/\hbar)], \tag{13}$$

which has to be solved self-consistently for $E_{\mu k}$ and $\Gamma_{\mu k}$. Consequently, $E_{\mu k}$ is the renormalized polariton band, and the renormalized polariton group velocity is obtained via $\tilde{v}_{g,\pm}(k_\parallel) = (1/\hbar)dE_{\pm k}/dk_\parallel$, which leads to

$$\tilde{v}_{g,\pm}(k_\parallel) = v_{g,\pm}(k_\parallel) + \frac{1}{\hbar}\frac{d}{dk_\parallel}\text{Re}\left[\Sigma_{\pm,k}(\tilde{E}_{\pm k}/\hbar)\right]. \tag{14}$$

The second term in the right-hand side of Eq. (14) characterizes the modification of the polariton group velocity due to polariton-phonon interaction. We hypothesize that this term is the main cause of the renormalization of v_g[4,21].

In most cases, Eq. (12) cannot be solved exactly, and approximations are needed to obtain the self-energy in a closed form. Here, we derive the leading contribution to polariton band renormalization using the standard tools of diagrammatic perturbation theory. The first-order self-energy is expressed as[32,34,35]

$$\Sigma^{(1)}_{\mu,k}(t) = i\zeta^2_{\mu k}\sum_{\nu,k'}\zeta^2_{\nu k'}\cdot D^{(0)}_{k-k'}(t)G^{(0)}_{\nu,k'}(t), \tag{15}$$

where $G^{(0)}_{\pm,k}(t) = -i\theta(t)e^{-i\omega_{\pm k}t}$ and $G^{(0)}_{\mathcal{D},k}(t) = -i\theta(t)e^{-i\omega_0 t}$ are the non-interacting Green functions of the polaritons and the dark excitons, respectively, and the low-temperature limit is taken because $\epsilon_{\mu k} \gg k_B T$. Furthermore, $D^{(0)}_{k-k'}(t)$ is the free phonon propagator under finite temperature, and is expressed as

$$D^{(0)}_q(t) = -i\sum_\alpha \frac{2c_\alpha^2}{N}[(1+\overline{n}_\alpha)e^{-i\omega_\alpha|t|} + \overline{n}_\alpha e^{i\omega_\alpha|t|}], \tag{16}$$

where $D^{(0)}_q(t)$ is independent of q, $\overline{n}_\alpha = 1/(e^{\beta\hbar\omega_\alpha} - 1)$ is the Bose-Einstein distribution function, and the bath modes are degenerate such that $\omega_{\alpha,q} = \omega_{\alpha,-q} = \omega_\alpha$. A diagrammatic representation for the polariton Green's functions and self-energies are provided in Supplementary Fig. 1. Eq. (15) is the Fan-Migdal self-energy[33], and when substituted in Eq. (14), leads to the following expression for the modified polariton bands

$$E^{(2)}_{\mu k} = \hbar\omega_{\mu k} + \zeta^2_{\mu k}\cdot\sum_{\nu,k'}\sum_\alpha \zeta^2_{\nu k'}\cdot\frac{2c_\alpha^2}{N}\cdot\Xi_{\mu k,\nu k'}(\omega_\alpha), \tag{17}$$

where $\Xi_{\mu k,\nu k'}(\omega_\alpha)$ is the real part of the polarizability and is given by

$$\Xi_{\mu k,\nu k'}(\omega_\alpha) = \text{Re}\left[\frac{1+\overline{n}_\alpha}{\omega_{\mu k} - \omega_{\nu k'} - \omega_\alpha + i\eta} + \frac{\overline{n}_\alpha}{\omega_{\mu k} - \omega_{\nu k'} + \omega_\alpha + i\eta}\right]. \tag{18}$$

A detailed derivation of Eq. (18) is provided in Supplementary Note 2. For continuous spectral density functions, the summation over the phonon modes α in Eq. (17) can be written as an integral in terms of $J(\omega)$ (see Supplementary Note 3). We note that the band modification can also be obtained directly from the total Hamiltonian using Rayleigh-Schrödinger perturbation theory[33], by treating $\hat{H}_{SB}$ as perturbative interactions that cause 2nd-order energy corrections (that scatter $|-,k\rangle$ to dark states then scatter back). This derivation is provided in Supplementary Note 2D, with the results identical to Eq. (17) (with $\eta = 0$).

In this work, we focus on the LP's v_g renormalization, which is dominated by scattering to the dark exciton states (a total of $N-\mathcal{M}$ of them), as opposed to scattering to the $\mathcal{M}$ LP and $\mathcal{M}$ UP states because $N-\mathcal{M} \gg 2\mathcal{M}$. Thus, one can explicitly perform the summation over k' that only includes the dark exciton contributions with $\sum_{k'} f(\omega_{\nu k'}) \approx (N-\mathcal{M}) f(\omega_0)$, and the $N-\mathcal{M}$ factor will cancel with $1/N$ in Eq. (17) under the large N limit. The validity of this approximation is further demonstrated numerically in Supplementary Fig. 2. This cancellation also indicates that in simulations, as long as one can keep $(N-\mathcal{M})/N \to 1$, one should expect the same converged results, and the detailed choice of N or $\mathcal{M}$ does not matter that much (assuming sufficient resolution of the polariton wavepacket in the spatial and k-space).

With the above considerations, the renormalized LP group velocity becomes

$$\tilde{v}_{g,-} = v_{g,-} + \frac{d}{dk_\parallel}\left[|C_k|^2 \sum_\alpha 2c_\alpha^2 \cdot \Xi_{-k,0}(\omega_\alpha)\right], \tag{19}$$

where the Hopfield coefficient $|C_k|^2$ is expressed as

$$|C_k|^2 = \sin^2\Theta_k = \frac{1}{2}\left[1 + \frac{\omega_k - \omega_0}{\sqrt{(\omega_k-\omega_0)^2 + 4Ng_k^2}}\right], \tag{20}$$

which characterizes the matter fraction of the LP. Furthermore, $\Xi_{-k,0}(\omega_\alpha)$ only considers the dark exciton contribution and is expressed as

$$\Xi_{-k,0}(\omega_\alpha) = \frac{\overline{n}_\alpha \cdot (\omega_\alpha - \Delta\omega_{-k})}{(\omega_\alpha - \Delta\omega_{-k})^2 + \eta^2} - \frac{1+\overline{n}_\alpha}{\omega_\alpha + \Delta\omega_{-k}}, \tag{21}$$

where $\Delta\omega_{-k} = \omega_0 - \omega_{-k} > 0$ is the energy gap between the dark exciton states and the LP band at $k_\parallel = \frac{2\pi}{NL}k$. Eq. (19) provides an analytic expression of the LP group velocity based on the current theory. It predicts that the magnitude of the v_g renormalization will depend linearly on λ [through c_α^2], and also predicts that v_g is sensitive to C_k and temperature [through $\overline{n}_\alpha$]. In Supplementary Fig. 3, we present the plot of the amplitude of v_g renormalization against the matter fraction $|C_k|^2$, and against the temperature, respectively. Further taking the $\eta \to 0$ limit of Eq. (21), one can analytically express Eq. (19) as

$$\begin{aligned} \Delta v_{g,-} &\equiv \tilde{v}_{g,-} - v_{g,-} \\ &= -\frac{d}{dk_\parallel}\left[|C_k|^2 \sum_\alpha 2c_\alpha^2 \omega_\alpha \frac{\Delta\omega_{-k}\cdot(2\overline{n}_\alpha+1)-\omega_\alpha}{\Delta\omega_{-k}^2 - \omega_\alpha^2}\right]. \end{aligned} \tag{22}$$

In most experiments, the LP initial excitation is in a region $\Delta\omega_{-k} \gg \omega_\alpha$, thus $\Xi_{-k,0}(\omega_\alpha)$ is negative. For a broad range of phonon frequencies, the high-frequency phonon makes a positive contribution to $\Xi_{-k,0}(\omega_\alpha)$, but the overall results should still be dominated by the low-frequency phonons, making $\Xi_{-k,0}(\omega_\alpha)$ negative. Note that Eq. (19) is only valid when dark excitons dominate the sum in Eq. (17). Nevertheless, one is able to derive simpler analytic answers from Eq. (17) or Eq. (19) under different regimes of spectral densities $J(\omega)$ or temperatures.

Mechanistic picture

We want to comment on the mechanistic picture suggested by Eqs. (22) and (17). The LP group velocity renormalization occurs mainly due to the presence of the dark states as a virtual scattering state. The transition from LP to all dark states, and scattering back to the LP ($|-,k\rangle \to |\mathcal{D}\rangle \to |-,k\rangle$) leads to the reduction of the group velocity, which can be understood as the perturbative energy correction up to second order. Indeed, the overall scaling of $\Delta v_{g,-} \propto 1/\Delta\omega_{-k}$. This scaling means that even with large light matter detunings, such that the dark states are never appreciably populated from the LP, these dark states still act like virtual states, such that their perturbative presence will lead to energy correction of LP and hence v_g renormalization. In this sense, we can classify the physical picture predicted by Eq. (22) as the super-exchange-like mechanism, where the dark exciton states act like virtual states to mediate the population transfer with LP. For small light-matter detuning (such as in ref. 3), the LP might be able to transfer the population to the dark states. Note that the typical super-exchange process describes indirect energy transfer to another state mediated by virtual states, rather than back to the initial state[36,37]. For a large light-matter detuning, dark states will only be virtually populated and thus will not be detected spectroscopically, as experimentally observed under resonant excitation of the LP in ref. 4. Supplementary Fig. 5 presents the polariton band structure and group velocity modification under different detunings, and Supplementary Fig. 6 presents a two-dimensional "heat map" of the detuning effect under different ω_c and $k_\parallel$. Furthermore, Supplementary Fig. 7 presents the population dynamics of the polariton and dark states obtained from Ehrenfest dynamics simulations under different detunings. We also note that the mechanism is akin to the Raman scattering process, which is evidenced by the expression of $\Xi_{\mu k,\nu k'}(\omega_\alpha)$ in Eq. (18). In fact, Eq. (17) is the Raman-type polarizability in the frequency domain, which is the well-known Kramers–Heisenberg–Dirac (KHD) expression[38–41], but now with temperature dependence (because the interaction is $\hat{H}_{SB}$, which is temperature dependent, and not the dipole interaction with the field in the original KHD expression). Supplementary Note 2D clearly shows how the $\hat{H}_{SB}$ term mediates the transition from LP to dark states and back to LP bands. As such, the v_g-renormalization can also be described as a phonon-mediated Raman-type scattering process, which is a non-resonant process. A schematic illustration is provided in Fig. 1b. Finally, the mechanism is also akin to the model used in the quantum relaxation process (see Chapter 9 of ref. 29).

Note that under the polariton representation, an alternative mechanistic picture could be phonon-mediated attractive interactions between polaritons and dark excitons, manifested by the negative energy correction in Eq. (17) (and one can further obtain an effective interacting polariton Hamiltonian via a Schrieffer–Wolff transformation[32,42,43], for example). In this sense, polariton attractions provide a backward drag force to the polariton wavefront and slow down the propagation. This mechanistic picture is consistent with the dark states manifold-mediated scattering effect discussed above. Note that the above-mentioned is just an interpretation, and the current theory or simulations do not explicitly consider the many-body interactions (such as exciton-exciton or polariton-polariton interactions).

We emphasize that the current theory predicts a less sensitive bath characteristic phonon frequency ω_f dependence of v_g. See Supplementary Fig. 8 for details. Nevertheless, increasing ω_f could lead to a more significant LP → DS population transfer, which breaks the equilibrium theory (See Supplementary Fig. 9). On the other hand, when increasing the light-matter detunings so that LP → DS population transfer is suppressed, Supplementary Fig. 10 shows that v_g is indeed less sensitive to ω_f. Furthermore, we emphasize that the polariton band modification expressed in Eq. (17), or approximately [c.f. Eq. (19)], $E^{(2)}_{-,k} \approx \left[|C_k|^2 \sum_\alpha 2c_\alpha^2 \cdot \Xi_{-k,0}(\omega_\alpha)\right]$ does not cause the shift of the optical signal[44]. For angle-resolved cavity photonic spectra, our results indicate that in optical measurements of the polariton dispersion, phonon coupling will only broaden the spectra, not change the peak frequency or band dispersion (see Supplementary Fig. 11). As such, $E^{(2)}_{-,k}$ is a unique quantity that renormalizes the group velocity, but does not directly influence linear optical signals. Our model thus closely matches experimental measurements that display no measurable renormalization of the polariton dispersion measured from linear reflectance or transmission spectra, but a large group velocity renormalization in nonequilibrium measurements of polariton propagation.

Numerical results

To quantitatively examine the accuracy of the above theory (Eq. (17), or the corresponding $\tilde{v}_{g,-}$), we perform quantum dynamics simulations for the GHTC model Hamiltonian using the Ehrenfest method[21], and verify various scaling relations and predictions made by the theory. For the system Hamiltonian, we chose the exciton energy $\hbar\omega_0 = 1.96$ eV, the cavity frequency $\hbar\omega_c = 1.90$ eV, and the collective light-matter coupling strength $\sqrt{N}g_c = 120$ meV. Details of the models and computations are provided in Supplementary Note 4, with a brief summary provided in the "Methods" section.

Figure 2 a presents the modified polariton band structure (Eq. (17)) with different λ. One observes that the modification of v_g increases as λ and the matter fraction increase. For the LP branch, the second term in Eq. (17) is negative, which effectively provides an attractive interaction between polaritons (mediated by phonons) and decreases the LP energy. Since $\zeta^2_{\mu k}$ is the matter fraction of the polariton branch, it is straightforward to see that as $k_\parallel$ increases, ζ^2_{-k} increases with a larger matter fraction, thus providing more modifications to the LP band. The modified polariton band structure consequently leads to polariton group velocity renormalization. Note that when both λ and $k_\parallel$ are large, the polariton dispersions bend down and have a negative slope (red and green curves in Fig. 2a), implying that $\tilde{v}_{g,-}$ becomes negative. This behavior is unphysical due to the breakdown of the perturbation theory used to derive Eq. (17). The quantum dynamics simulations[21] suggest that under this regime, the transport will become diffusive with a very small v_g. For the results presented later, we only focus on the region of $k_\parallel \geq 0$ predicted by the analytic theory in Eq. (19).

Figure 2b presents the LP group velocity as a function of the bare LP energies (see the black curve in Fig. 2a) and for different λ, where the theoretical results using Eq. (17) are compared to quantum dynamics simulations (open circles). One sees that as λ increases, the magnitude of the group velocity renormalization increases (from the blue curve to the green curve), further deviating from the derivative of the LP band, v_g (black solid curve). Furthermore, as the LP energy increases, the matter character of the LP state $|C^2_k|$ also increases, which further reduces the group velocity. For all cases, the theory agrees very well with the numerical simulations for small λ (<12 meV). However, for larger λ, the polariton-phonon interaction enters the non-perturbative regime, and the first-order self-energy level theory in Eq. (17) becomes inadequate. As a result, the theory gradually deviates from numerical simulations, as expected. Nevertheless, the theory describes the overall semi-quantitative trend of the data from the simulation.

Figure 2c presents the scaling relation of the LP group velocity $\tilde{v}_{g,-}$ (c.f. Eq. (19)) as a function of λ, which characterizes the modification to the LP group velocity by the polariton-phonon interaction. Importantly, the theory in Eq. (19) predicts that this renormalization magnitude is proportional to c^2_α and thus $|\Delta v_{g,-}| = |\tilde{v}_{g,-} - v_{g,-}| \propto \lambda$. Figure 2c presents $\tilde{v}_{g,-}$ versus λ at different LP energies. We observe that $\tilde{v}_{g,-}$ scales linearly with λ, and the slope increases as the matter fraction increases. It is clear from Eq. (17) that the polariton band structure (or group velocity) modification is proportional to λ due to its quadratic dependence on c_α. The results obtained from quantum dynamics simulations agree quite well with the theory, especially for cases with small λ and matter fractions. As λ and matter fraction increase, the Ehrenfest results gradually deviate from the theory and show a nonlinear dependence on λ, due to non-perturbative effects; see the $\epsilon_{-k} = 1.84$ eV (shallow green) curve for example. Nevertheless, the semi-quantitative trend is always captured by the theory, and we stress that there are no free parameters in the current theory. Furthermore, our quantum dynamics simulation is based on the Ehrenfest MQC approximation, which may lead to inaccurate results when λ is large. Future efforts are needed to evaluate v_g in the large λ regime using more accurate quantum dynamics approaches.

Figure 2d presents the temperature dependence of the polariton group velocity renormalization. Figure 2d presents $\tilde{v}_{g,-}$ versus T at LP energy $\epsilon_{-k} = 1.86$ eV and $\lambda = 6$ meV. From a theoretical standpoint, the temperature dependence is mainly carried by the Bose–Einstein distribution function in Eq. (17), which is nonlinear in T. In particular, under the high-temperature limit ($\hbar\omega_\alpha \ll k_B T$ for all ω_α), the Bose-Einstein distribution function can be approximated as

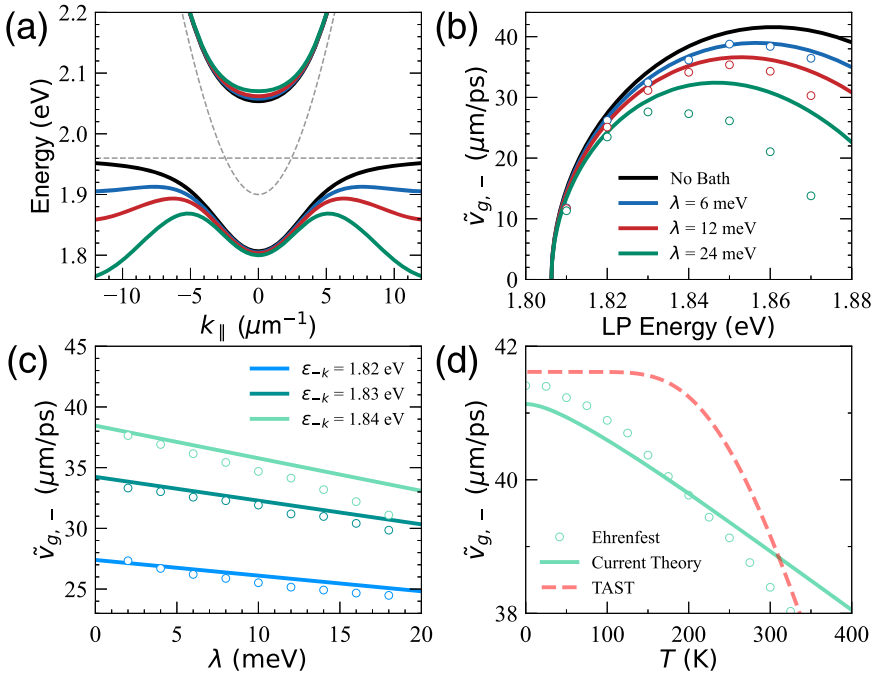

Fig. 2 | Polariton energy and group velocity renormalization due to polariton-phonon interaction. a Modified polariton band structure under different λ. **b** Group velocity of the LP branch $\tilde{v}_{g,-}$ as a function of the bare LP energy (black curve in (**a**)). under different λ. **c** Scaling relation of the LP group velocity $\tilde{v}_{g,-}$ with λ. **d** Temperature-dependence of the LP group velocity $\tilde{v}_{g,-}$ at LP energy $\epsilon_{-k} = 1.86$ eV and $\lambda = 6$ meV. Theoretical results using Eq. (17) (solid lines) are compared to Ehrenfest dynamics simulations (open circles).

$\overline{n}_\alpha \approx k_B T/(\hbar\omega_\alpha) \propto T$. As a result, the modification of the polariton band structure (or group velocity) is proportional to T. At temperatures near 300 K, the parameters we used satisfy the high-temperature limit; thus $\Delta v_{g,-}$ scales linearly with T. In the Ehrenfest dynamics simulations, the nuclear quantum effect comes from the initial Wigner distribution of the nuclear thermal density only, and the exciton-phonon dynamics beyond the quantum-classical limit are not captured. Considering this, the deviation between Ehrenfest dynamics and the theory is likely due to the inaccuracy of Ehrenfest dynamics at very low temperatures, as we expect that our analytic theory should be accurate under the low λ, even when $T \to 0$ limits (because there is no additional approximations related to the temperature dependence factor in Eq. (21)). Nevertheless, both the current theory (solid green line) and the numerical simulation agree reasonably well across all temperature regimes. Overall, the theory and simulations predict that $v_{g,-}$ decreases as T increases. This is because when T increases, the phonon fluctuations cause transitions from the LP band to the dark exciton states, thus reducing the group velocity. We also want to emphasize that there is no free parameter in the current theory to predict the temperature dependence.

Note that a phenomenological expression has previously been proposed based on the TAST[6], due to scattering from $|-_k\rangle$ to the dark states, resulting in the following expression for the group velocity renormalization

$$\tilde{v}_{g,-} = \frac{v_{g,-}}{1 + G \cdot e^{-\beta\hbar\Delta\omega_{-k}}}, \tag{23}$$

where G is a free parameter. See Supplementary Note 5, as well as Supplementary Information S3 in ref. 6 for further details. The TAST is based on the idea that transport depends on the proportion of time the system spends in the LP band relative to the dark states, resulting in a temperature-dependent modification of v_g that is sensitive to the energy gap $\Delta\omega_{-k}$. Although the TAST makes intuitive sense (and aligns with findings from our microscopic theory), we found that Eq. (23) does not give the correct temperature dependence when G is treated as a temperature-independent parameter. In Fig. 2, the result from TAST is plotted as the red dashed curve, with a fitting parameter $G = 3.0$ to reproduce the correct value of $\tilde{v}_{g,-}$ at $T = 300$ K. One sees that it does not give the correct T-dependence across a broad range of temperatures unless one further chooses a T-dependent G parameter. The reason TAST fails to reproduce an accurate T-dependence is because the expression from TAST scales as $1/(1 + e^{-\beta\hbar\Delta\omega_{-k}})$, whereas the microscopic theory in Eq. (19) posits that the temperature dependence is $\overline{n}_\alpha \approx e^{-\beta\hbar\omega_\alpha}$ under the low-temperature limit when $\hbar\omega_\alpha \gg k_B T$, and $\overline{n}_\alpha \approx k_B T/(\hbar\omega_\alpha)$ under the high-temperature limit when $\hbar\omega_\alpha \ll k_B T$. Additionally, TAST assumes that the transition between the LP band and dark exciton states follows Boltzmann statistics, whereas, in our current theory, the phonons obey Bose-Einstein statistics, which mediate the (virtual) transitions between the LP band and the dark states. Our microscopic theory also predicts that $\Delta v_{g,-}$ should depend on $\Delta\omega_{-k}$, but this dependence (in Eq. (19)) is not in the Boltzmann factor. As such, at a low temperature when $k_B T \ll \hbar\Delta\omega_{-k}$ (for a large energy difference between LP and dark excitons), but still has $k_B T \sim \hbar\omega_\alpha$ (for low-frequency acoustic phonon α), TAST predicts that there is no renormalization, and the current theory predicts that there will be a finite magnitude of renormalization (see Fig. 2D for $T < 150$ K). Preliminary experimental evidence of such a low-temperature v_g renormalization can be found in Fig. 3c in ref. 13. On the other hand, if one wants to choose the mechanistic interpretation based on Eq. (23), then our current theory will give a precise expression of how G should depend on temperature, which is $G = (e^{\beta\hbar\Delta\omega_{-k}}/\tilde{v}_{g,-})\frac{d}{dk_\parallel}\left[|C_k|^2 \sum_\alpha 2c_\alpha^2 \cdot \Xi_{-k,0}(\omega_\alpha)\right]$, see details in Supplementary Note 5. In that sense, we view our current theory as a more general, microscopic one compared to TAST.

We developed a microscopic theory that successfully explains the renormalization of polariton group velocity due to polariton-phonon interactions. We analyze a theoretical model based on the GHTC Hamiltonian, which comprises N identical copies of molecular systems consisting of excitons and phonons that are collectively coupled to $\mathcal{M}$ cavity modes, which satisfy some dispersion relation. The theory uses a diagrammatic perturbative treatment of the equilibrium Green's function of the polaritons, revealing how exciton-phonon interactions renormalize the LP band and thus reduce the group velocity in polariton transport. Crucially, the theory captures the λ and T dependence of the v_g renormalization magnitude and semi-quantitatively agrees with results from quantum dynamics simulations. We emphasize that there is no free parameter in our microscopic theory, and every quantity is derived from the microscopic light-matter interaction Hamiltonian.

We expect the theory will eventually break down with increasing λ and matter fraction, such that the system enters into the non-perturbative regime. However, for $\lambda \le k_B T$, the analytic theory almost quantitatively agrees with the numerical results. Although the theory does not capture transient non-equilibrium dynamical behaviors in the short-time regime, it yields semi-quantitatively accurate answers compared to numerical simulations that do include all transient non-equilibrium effects. This strongly suggests that the LP v_g renormalization is largely dictated by the renormalization of the LP band due to phonons and is less sensitive to the transient dynamics.

Our theory yields several predictions regarding the scaling relation with matter fraction $|C_k|^2$, phonon bath reorganization energy λ, temperature, etc., and these have been verified through our quantum dynamics simulations. These predictions can, in principle, be verified with experiments[3,4,6]. The theory is simple enough to be extended to multidimensional systems with multiple dispersive matter bands and phonons, such as semiconductor materials. It is also feasible to implement our theory along with ab initio simulations[33].

Methods

Numerical evaluation of Eq. 17

We assume a Drude–Lorentz form for the phonon bath spectral density $J(\omega) = \frac{\pi}{\hbar}\sum_\alpha c_\alpha^2 \delta(\omega - \omega_\alpha) = 2\lambda\omega_f\omega/(\omega^2 + \omega_f^2)$, where λ is the reorganization energy, and ω_f is the bath characteristic frequency. We adopt an efficient and commonly used type of bath discretization procedure[45], which discretizes the spectral density with equal intervals in λ (instead of in frequency), with

$$\omega_\alpha = \omega_f \tan\left[\frac{\pi}{2}\left(1 - \frac{\alpha}{N_b + 1}\right)\right], \quad c_\alpha = \sqrt{\frac{\lambda\omega_\alpha}{N_b + 1}}, \tag{24}$$

where $\alpha = 1, \cdots, N_b$, and N_b is the number of bath modes. Here $N_b = 10^4$ is used to evaluate Eq. (17) to generate converged results, and the infinitesimal imaginary term in Eq. (18) is taken as $\eta = 1$ meV. The value of $\tilde{v}_{-,g}$ is directly obtained by numerically differentiating $E_{\mu k}^{(2)}$ in Eq. (17). Note that one can adopt a smaller η value in numerical calculations, but it then requires an even larger N_b to reach convergence.

Quantum dynamics simulations

We use the mean-field Ehrenfest dynamics[21] to propagate the quantum dynamics of polariton transport. The transport dynamics mainly occur in the single excitation subspace, defined as follows

$$|E_n\rangle = |e_n\rangle \bigotimes_{m\neq n} |g_m\rangle \bigotimes_k |0_k\rangle \tag{25}$$

$$|k\rangle = |G\rangle \bigotimes_{k'\neq k} |0_{k'}\rangle \otimes |1_k\rangle, \tag{26}$$

where $|E_n\rangle$ is the singly excited state for the n_{th} molecule located at x_n, $|k\rangle$ is the one-photon-dressed ground state with wave-vector $k_\parallel = \frac{2\pi}{NL}k$, and L is the inter-molecular spacing, which is set to be L = 40 Å. Furthermore, $|G\rangle = \bigotimes_n |g_n\rangle \bigotimes_\alpha |0_k\rangle$ represents the common ground state for the hybrid system. We describe the time-dependent quantum state in the exciton-photon subspace as

$$|\psi(t)\rangle = \sum_n^N c_n(t)|E_n\rangle + \sum_k c_k(t)|k\rangle, \tag{27}$$

where $c_n(t)$ and $c_k(t)$ are the excitonic and photonic expansion coefficients, respectively. The polariton quantum dynamics for $|\psi(t)\rangle$ is propagated by solving the time-dependent Schrödinger equation (TDSE),

$$i\hbar\frac{\partial}{\partial t}|\psi(t)\rangle = \hat{H}_{\text{Q}}(\mathbf{R})|\psi(t)\rangle, \tag{28}$$

where $\hat{H}_{\text{Q}} = \hat{H}_{\text{S}} + \hat{H}_{\text{SB}}(\mathbf{R})$. The bath nuclear DOF $\mathbf{R}$, on the other hand, is propagated classically using Hamilton's equations of motion (EOM), governed by the time-dependent mean-field force

$$\mathbf{F} = -\nabla_{\mathbf{R}}\left[\left\langle\psi(t)|\hat{H}_{\text{SB}}(\mathbf{R})|\psi(t)\right\rangle + h_{\text{B}}(\mathbf{R})\right]. \tag{29}$$

The polariton group velocity $\bar{v}_g$ is computed by tracking the wavefront of the LP polariton wave packet using the same method reported in previous works[4,21], with details provided in Supplementary Note 4. Example spatial distribution of the polariton wavepacket at different time and the extraction of the group velocity are shown in Supplementary Fig. 4, with detailed fitting parameters in Supplementary Table III.

Simulation details

For all quantum dynamics simulations, we use $N = 10^4$ molecules and $\mathcal{M} = 10^2$ cavity modes, keeping the ratio of $N/\mathcal{M} \approx 35$. More details about the precise number of molecules and modes for each parameter regime explored in Fig. 2 are provided in Supplementary Note 4 (see Supplementary Table I and Supplementary Table II). A total of $N_b = 35$ phonon modes were sampled based on the same equal-λ procedure mentioned above. The total light-matter coupling strength is set to $\sqrt{N}g_{\text{c}} = 120$ meV. All results are obtained with an ensemble of 500 independent trajectories. Convergence tests are performed with up to 1000 trajectories. The nuclear time step is $\Delta t = 2.5$ fs, where during each nuclear propagation, there are 100 electronic propagation steps with a time step $dt = 0.025$ fs. The nuclear EOM is numerically integrated with the velocity verlet algorithm, and the TDSE is solved with the Runge-Kutta-4 algorithm.

Data availability

The data generated in this study have been deposited in https://github.com/Okita0512/Polariton-Transport.

Code availability

The source code for the Ehrenfest quantum dynamics method used in this study is available at https://github.com/benxkchng/Polariton-Transport-Ehrenfest. The source code for producing all the figures in the main text and the supplementary notes is available at https://github.com/Okita0512/Polariton-Transport.

References

1. Hou, S. et al. Ultralong-range energy transport in a disordered organic semiconductor at room temperature via coherent exciton-polariton propagation. *Adv. Mater.* **32**, https://doi.org/10.1002/adma.202002127 (2020).
2. Berghuis, A. M. et al. Controlling exciton propagation in organic crystals through strong coupling to plasmonic nanoparticle arrays. *ACS Photonics* **9**, 2263 (2022).
3. Pandya, R. et al. Tuning the coherent propagation of organic exciton-polaritons through dark state delocalization. *Adv. Sci.* **9**, 2105569 (2022).
4. Xu, D. et al. Ultrafast imaging of polariton propagation and interactions. *Nat. Commun.* **14**, 681–708 (2023).
5. Cheng, S. W. et al. Optical imaging of ultrafast phonon-polariton propagation through an excitonic sensor. *Nano Lett.* **23**, 9936 (2023).
6. Balasubrahmaniyam, M. et al. From enhanced diffusion to ultrafast ballistic motion of hybrid light-matter excitations. *Nat. Mater.* **22**, 338 (2023).
7. Sandik, G., Feist, J., García-Vidal, F. J., and Schwartz, T. Cavity-enhanced energy transport in molecular systems. *Nat. Mater.* https://doi.org/10.1038/s41563-024-01962-5 (2024).
8. Liu, B., Huang, X., Hou, S., Fan, D. & Forrest, S. R. Photocurrent generation following long-range propagation of organic exciton–polaritons. *Optica* **9**, 1029 (2022).
9. Gather, M. C., Köhnen, A. & Meerholz, K. White organic light-emitting diodes. *Adv. Mater.* **23**, 233 (2011).
10. Reineke, S. et al. White organic light-emitting diodes with fluorescent tube efficiency. *Nature* **459**, 234 (2009).
11. Reineke, S., Thomschke, M., Lüssem, B. & Leo, K. White organic light-emitting diodes: Status and perspective. *Rev. Mod. Phys.* **85**, 1245 (2013).
12. Rozenman, G. G., Akulov, K., Golombek, A. & Schwartz, T. Long-range transport of organic exciton-polaritons revealed by ultrafast microscopy. *ACS Photonics* **5**, 105–110 (2018).
13. Hong, Y., Xu, D. & Delor, M. Exciton delocalization suppresses polariton scattering. https://doi.org/10.48550/arXiv.2506.08770 (2025).
14. Schachenmayer, J., Genes, C., Tignone, E. & Pupillo, G. Cavity-enhanced transport of excitons. *Phys. Rev. Lett.* **114**, 196403 (2015).
15. Zhou, Z., Chen, H.-T., Sukharev, M., Subotnik, J. E. & Nitzan, A. Nature of polariton transport in a Fabry-Perot cavity. *Phys. Rev. A* **109**, 033717 (2024).
16. Suyabatmaz, E. & Ribeiro, R. F. Vibrational polariton transport in disordered media. *J. Chem. Phys.* **159**, 034701 (2023).
17. Aroeira, G. J. R., Kairys, K. T. & Ribeiro, R. F. Coherent transient exciton transport in disordered polaritonic wires. *Nanophotonics* **13**, 2553 (2024).
18. Engelhardt, G. & Cao, J. Polariton localization and dispersion properties of disordered quantum emitters in multimode microcavities. *Phys. Rev. Lett.* **130**, 213602 (2023).
19. Tutunnikov, I., Qutubuddin, M., Sadeghpour, H. R. & Cao, J. Characterization of polariton dynamics in a multimode cavity: noise-enhanced ballistic expansion. Preprint at https://doi.org/10.48550/arXiv.2410.11051 (2024).
20. Sokolovskii, I., Tichauer, R. H., Morozov, D., Feist, J. & Groenhof, G. Multi-scale molecular dynamics simulations of enhanced energy transfer in organic molecules under strong coupling. *Nat. Commun.* **14**, 6613 (2023).
21. Chng, B. X. K., Mondal, M. E., Ying, W. & Huo, P. Quantum dynamics simulations of exciton polariton transport. *Nano Lett.* **25**, 1617 (2025).
22. Tichauer, R. H., Sokolovskii, I. & Groenhof, G. Tuning the coherent propagation of organic exciton-polaritons through the cavity Q-factor. *Adv. Sci.* **10**, 2302650 (2023).
23. Herrera, F. & Spano, F. C. Theory of nanoscale organic cavities: the essential role of vibration-photon dressed states. *ACS Photonics* **5**, 65 (2018).
24. Qiu, L. et al. Molecular polaritons generated from strong coupling between CdSe nanoplatelets and a dielectric optical cavity. *J. Phys. Chem. Lett.* **12**, 5030 (2021).

25. Mandal, A. et al. Theoretical advances in polariton chemistry and molecular cavity quantum electrodynamics. *Chem. Rev.* **123**, 9786 (2023).
26. Taylor, M. A. D., Mandal, A. & Huo, P. Light-matter interaction Hamiltonians in cavity quantum electrodynamics. *Chem. Phys. Rev.* **6**, 011305 (2025).
27. del Pino, J., Feist, J. & Garcia-Vidal, F. J. Quantum theory of collective strong coupling of molecular vibrations with a microcavity mode. *New J. Phys.* **17**, 053040 (2015).
28. Caldeira, A. & Leggett, A. Quantum tunnelling in a dissipative system. *Ann. Phys.* **149**, 374 (1983).
29. Nitzan, A. *Chemical Dynamics in Condensed Phases* (Oxford, New York, 2006).
30. Deng, H., Haug, H. & Yamamoto, Y. Exciton-polariton Bose-Einstein condensation. *Rev. Mod. Phys.* **82**, 1489 (2010).
31. Chng, B. X. K. et al. Mechanism of molecular polariton decoherence in the collective light-matter couplings regime. *J. Phys. Chem. Lett.* **15**, 11773 (2024).
32. Mahan, G. D. *Many-Particle Physics* 3rd edn (Springer New York, NY, 2000).
33. Giustino, F. Electron-phonon interactions from first principles. *Rev. Mod. Phys.* **89**, 015003 (2017).
34. Robinson, P. J., Dunn, I. S. & Reichman, D. R. Cumulant methods for electron-phonon problems. I. Perturbative expansions. *Phys. Rev. B* **105**, 224304 (2022).
35. Robinson, P. J., Dunn, I. S. & Reichman, D. R. Cumulant methods for electron-phonon problems. II. The self-consistent cumulant expansion. *Phys. Rev. B* **105**, 224305 (2022).
36. Berkelbach, T. C., Hybertsen, M. S. & Reichman, D. R. Microscopic theory of singlet exciton fission. II. Application to pentacene dimers and the role of superexchange. *J. Chem. Phys.* **138**, 114103 (2024).
37. Hu, Y. & Mukamel, S. Superexchange and electron transfer in the photosynthetic reaction center. *Chem. Phys. Lett.* **160**, 410 (1989).
38. Kramers, H. A. & Heisenberg, W. Über die streuung von strahlung durch atome. *Z. Phys.* **31**, 681–708 (1925).
39. Dirac, P. A. M. The quantum theory of the emission and absorption of radiation. *Proc. R. Soc. Lond. A* **114**, 243–265 (1927).
40. Dirac, P. A. M. The quantum theory of dispersion. *Proc. R. Soc. Lond. A* **114**, 710–728 (1927).
41. Tannor, D. J. *Introduction to Quantum Mechanics: A Time-Dependent Perspective* (University Science Book, 2006).
42. Schrieffer, J. R. & Wolff, P. A. Relation between the Anderson and Kondo Hamiltonians. *Phys. Rev.* **149**, 491 (1966).
43. Bravyi, S., DiVincenzo, D. P. & Loss, D. Schrieffer-Wolff transformation for quantum many-body systems. *Ann. Phys.* **326**, 2793 (2011).
44. Herrera, F. & Spano, F. C. Absorption and photoluminescence in organic cavity QED. *Phys. Rev. A* **95**, 053867 (2017).
45. Bose, A. & Makri, N. Non-equilibrium reactive flux: a unified framework for slow and fast reaction kinetics. *J. Chem. Phys.* **147**, 152723 (2017).

Acknowledgements

This work was supported by the Air Force Office of Scientific Research under AFOSR Award No. FA9550-23-1-0438, the National Science Foundation Award under Grant No. CHE-2244683, as well as by the University of Rochester PumpPrimer II funding. M.D. acknowledges support from the Office of Naval Research under Grant No. N00014-25-1-2079. W.Y. appreciates the support of the Moses Passer Graduate Fellowship at the University of Rochester, as well as the ACS Chemical Computing Group Excellence Award for Graduate Students. P.H. appreciates the support of the Cottrell Scholar Award (a program by the Research Corporation for Science Advancement). We appreciate valuable discussions and comments from Arkajit Mandal. Computing resources were provided by the Center for Integrated Research Computing (CIRC) at the University of Rochester.

Author contributions

All authors designed the research. W.Y. and P.H. conducted theoretical derivations. W.Y. performed numerical evaluations of the theoretical expressions, B.X.K.C. performed the quantum dynamics simulations of polariton transport. M.D. and P.H. developed the mechanistic picture of group velocity re-normalization. W.Y., B.X.K.C., M.D., and P.H. wrote the manuscript.

Competing interests

The authors declare no competing interests.

Additional information

Supplementary information The online version contains supplementary material available at https://doi.org/10.1038/s41467-025-62276-x.

Correspondence and requests for materials should be addressed to Pengfei Huo.

Peer review information *Nature Communications* thanks Hsing-Ta Chen, Zeyu Zhou, and the other anonymous reviewer(s) for their contribution to the peer review of this work. A peer review file is available.